REACTION THEORIES FOR EXOTIC NUCLEI

Probing single-particle structures in rare nuclei

J.A. TOSTEVIN
Department of Physics
School of Electronics and Physical Sciences
University of Surrey
Guildford, Surrey GU2 7XH, U.K.

Abstract. Theoretical few-body reaction methods are discussed. Particular attention is given to approximate methods which use the adiabatic and eikonal approximations and which then make transparent the ingredients from reaction dynamics and nuclear structure to the calculations. Their applications to single-nucleon knockout reactions and to single particle spectroscopy are then discussed and examples of recent analyses are presented.

1. Introduction

With the advent of radioactive ion beam physics there has been a resurgence of interest in quantitative theories of nuclear reactions. Short lived exotic nuclei, in the form of low intensity secondary radioactive ion beams (RIBs) produced in nuclear fragmentation reactions, are now studied using a variety of secondary reactions in an attempt to understand their bulk properties and more detailed structures. The focus of these two lectures is:

> How can we learn about single particle structures in such exotic nuclei from reaction studies?

That is, how can we relate experimental observables, such as single-nucleon removal cross sections, or their distribution as a function of the final state fragment momenta, to properties of nuclear many-body wave functions Φ_A? More specifically, how can we deduce the removed nucleons' single particle (sp) configurations $\phi_{\ell j}$ and the associated occupancies or spectroscopic factors for these states? My emphasis here, because of the data available, is on the spectroscopy of exotic light neutron-rich nuclei with energies of a few 10s of MeV per nucleon, as produced at the facilities at the NSCL,

GANIL and at RIKEN. The methods discussed are also highly applicable to RIBs at yet higher energies, such as are produced at the GSI.

In the following, the methods and approximations currently used are introduced. These enable practical but approximate calculations of the wave functions of interacting systems and of the corresponding reaction observables. The selection of the correct approach requires an awareness of the reaction time scales and mechanisms involved which, in turn, depend on the nature of the nuclei involved, their charge, mass, and on their interactions.

The ordering, distribution of sp strength, and occupation of nucleonic single-particle states in nuclei is fundamental to their structure and stability. Experimental verification of such structures is also vital to test shell model and other many-body theoretical structure predictions away from the stable nuclei. With current low intensity RIBs however most traditional sp spectroscopic tools, such as the $(e, e'p)$ [1], (p, p'), and single-nucleon transfer reactions [2], are still very demanding [3, 4, 5, 6] or not yet available experimentally. The challenge for reaction theorists has been the new regimes of weak nuclear binding near the driplines, such as the halo states, and the availability, in the most part, of inclusive rather than exclusive reaction data.

Unlike structure methods, there are no practical true many-body reaction theories. Reaction methods can at most calculate approximate solutions of a *few-body* Schrödinger equation with *effective* interactions between the assumed few-bodies, usually individual nucleons and/or clusters of many nucleons.

The challenge for spectroscopy is therefore to develop methods which permit both the structure and reaction dynamics aspects of the problem to be treated with comparable rigour. There is little value in using detailed many-body wave functions as input to inappropriate or over simplistic reaction theory, and vice versa. This often demands that experimental choices of energies, targets, reactions and detection geometries be made which permit the use of appropriate theoretical approximations and which then make the required structure and reaction inputs more transparent. Our emphasis on sp spectroscopy suggests the use of (direct) reactions in which the projectile suffers minimal rearrangement in the collision – ideally exciting just a single nucleon, if possible [7, 8]. We concentrate here on single-nucleon removal from the projectile.

2. Few-body models: concepts

For orientation we will consider the scattering of a two-body projectile. The projectile's two constituents $j = c, v$, initially bound, will be thought of as a heavy nuclear core c and a light valence particle v, typically a nucleon.

These projectiles, with ground state wave function ϕ_0, are incident with energy E and react with or scatter from a target nucleus t. It is assumed, to be definite, that the projectile supports only one bound state. The constituents of the projectile interact with the target through complex effective interactions V_{jt}, often taken as phenomenological optical potentials fitted to experimental data or, alternatively, which are calculated from theoretical multiple scattering or folding models. For example, at the energies of principal interest to fragmentation beams, 50 MeV/nucleon and above, these two-body interactions can be estimated from the constituent particle and target densities and an approximate effective nucleon-nucleon (NN) interaction t_{NN} by the double-folding integral [9, 10]

$$V_{jt}(r_j) = \int d\vec{r}_1 \int d\vec{r}_2 \, \rho_j(r_1)\rho_t(r_2)t_{NN}(\vec{r}_j + \vec{r}_2 - \vec{r}_1) \ . \qquad (1)$$

If the particles are charged then of course the V_{jt} must include the appropriate Coulomb interactions also. We assume the potentials are central. We denote by $\vec{r}$ the relative coordinate of c and v in the projectile and by $\vec{R}$ the target-projectile centre of mass (c.m.) separation. When needed the z–axis will be chosen along the incident projectile beam direction.

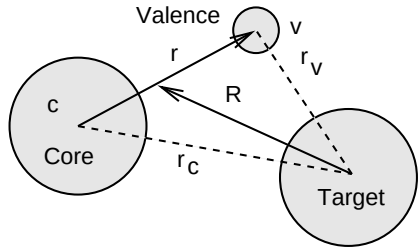

Figure 1. Coordinates used for a two-body projectile-target problem.

The Schrödinger equation satisfied by the scattering wave function $\Psi^{(+)}_{\vec{K}}$, when the projectile is incident with wave vector $\vec{K}$ in the c.m. frame, is

$$\left[T_R + U(\vec{r}, \vec{R}) + H_p \ - \ E \right] \Psi^{(+)}_{\vec{K}}(\vec{r}, \vec{R}) = 0 \ \ , \qquad (2)$$

Here H_p is the projectile's internal Hamiltonian, T_R is the projectile's c.m. kinetic energy operator and $U(\vec{r}, \vec{R})$ is the total interaction between the projectile and the target. ϕ_0 is an eigenstate of H_p with energy $-\varepsilon_0$. In general H_p will also generate an excited bound and continuum states spectrum. The few-body model approach is to solve as best one can the Schrödinger

equation (2) for $\Psi^{(+)}_{\vec{K}}$ with the incident wave boundary condition

$$\Psi^{(+)}_{\vec{K}}(\vec{r},\vec{R}) = e^{i\vec{K}\cdot\vec{R}}\,\phi_0(\vec{r}) \;+\; \text{outgoing waves} \quad . \tag{3}$$

In such an approach we note that ϕ_0 appears *only* as part of the incident boundary condition. In general therefore the connection between projectile structure, the solution $\Psi^{(+)}_{\vec{K}}$, and the reaction observables is very subtle and largely hidden. Before dealing with (approximate) solutions of this few-body dynamical problem we recall some important results from elementary (two-body) scattering theory, relevant to describing the scattering of each constituent, in isolation, from the target.

3. Results from scattering theory

3.1. THE PARTIAL WAVE S–MATRIX

Consider the scattering of two point-particles with relative energy E in their c.m. frame and which interact through a potential $V(r)$. If their reduced mass is μ then they have relative momentum $\hbar k = \sqrt{2\mu E}$. It is well known that the solution of the scattering wave function $\psi^{(+)}_{\vec{k}}(\vec{r})$ is usually carried out by partial wave expansion. The asymptotic form of the relative motion radial wave function, when the pair have relative orbital angular momentum ℓ, is

$$u_\ell(r) \to \frac{i}{2}\left[H^-_\ell(kr) - S_\ell H^+_\ell(kr)\right] \quad , \tag{4}$$

where the $H^\pm_\ell$ denote incoming $(-)$ and outgoing $(+)$ waves. Significantly, the partial wave S–matrix S_ℓ is the amplitude of the outgoing wave, and so $|S_\ell|^2$ is the probability that in a state with orbital motion ℓ the particles survive the collision and emerge from the reaction region. If $V(r)$ is complex, to account for open reaction channels, then of course $|S_\ell|^2 \leq 1$. If the mass of the particles or their energy is high, such that many ℓ contribute, then a semi-classical description in which the discrete ℓ are replaced by the continuous impact parameters b, where $\ell \approx kb$ (actually $\ell + 1/2 = kb$) can also be very accurate. $|S(b)|^2$ has the same interpretation as $|S_\ell|^2$, being unity for b larger than the interaction radius (transmission) and small for b smaller than the interaction radius (absorption). All reaction cross sections can be deduced from either of these orbital S–matrices, eg. the elastic and reaction cross sections

$$\sigma_{el} \;=\; \frac{\pi}{k^2}\sum_{\ell=0}^{\infty}(2\ell+1)|1-S_\ell|^2 \;\approx \int d\vec{b}|1-S(b)|^2 \quad , \tag{5}$$

$$\sigma_R \;=\; \frac{\pi}{k^2}\sum_{\ell=0}^{\infty}(2\ell+1)[1-|S_\ell|^2] \approx \int d\vec{b}[1-|S(b)|^2] \quad , \tag{6}$$

where $d\vec{b} = 2\pi b db$ denotes integration over all impact parameters.

3.2. EIKONAL THEORY FOR POINT PARTICLES

Less familiar is the (approximate) semi-classical eikonal solution of the Schrödinger equation [11, 12]. In common with other semi-classical approaches, the method is useful when the incident particle wave number k is large and so has a short wavelength compared with typical distances over which the potential $V(r)$ changes appreciably. Now the scattering wave function is written $\psi^{(+)}_{\vec{k}}(\vec{r}) = \exp(i\vec{k}\cdot\vec{r})\omega(\vec{r})$, a product of the incident plane-wave state with an as yet unknown modulating function $\omega(\vec{r})$, which carries all information of the effects of $V(r)$. Substituting this product form in the Schrödinger equation yields

$$\left[2i\nabla\omega(\vec{r})\cdot\vec{k} - \frac{2\mu}{\hbar^2}V(r)\omega(\vec{r}) + \nabla^2\omega(\vec{r})\right]\exp(i\vec{k}\cdot\vec{r}) = 0 \ , \tag{7}$$

and the eikonal approximation neglects the term in $\nabla^2\omega$ which, for large k and slow potential variation, should be small compared to $2\nabla\omega\cdot\vec{k}$. With the z–axis along $\vec{k}$, ω satisfies the first order equation

$$\frac{\partial\omega}{\partial z} = -\frac{i}{\hbar v}\,V(r)\omega(\vec{r}) \tag{8}$$

with solution, at impact parameter $b = \sqrt{x^2+y^2}$, of

$$\omega(\vec{r}) = \exp\left\{-\frac{i}{\hbar v}\int_{-\infty}^{z} V(\sqrt{b^2+z'^2})dz'\right\} \quad . \tag{9}$$

Here $v = \hbar k/\mu$ is the classical incident velocity in the c.m. frame. Note that our neglect of the curvature term $\nabla^2\omega$ has assumed that ω can be estimated accurately by assuming the scattered particle traverses a straight line path through $V(r)$ at impact parameter b.

The result we want is that, following the collision at impact parameter b, the wave function is (for $z \to \infty$)

$$\psi^{eik}_{\vec{k}}(\vec{r}) \to S(b)e^{i\vec{k}\cdot\vec{r}} = \exp\left\{-\frac{i}{\hbar v}\int_{-\infty}^{\infty} V(\sqrt{b^2+z'^2})dz'\right\} e^{i\vec{k}\cdot\vec{r}} \ , \tag{10}$$

where $S(b)$, the amplitude of the forward going scattered wave, is the eikonal approximation to the elastic scattering S–matrix. This can be evaluated rather simply as a one dimensional integration through the potential. Much more importantly, this simple product structure of the eikonal wave function will be shown to generalise to the case of few-body projectiles and will be used in the following.

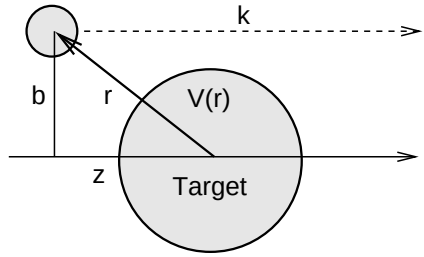

Figure 2. A straight line trajectory through $V(r)$ is assumed in the eikonal approximation

4. Breakup of composite systems

We now return to discussion of the case of a few-body projectile. The Schrödinger equation for the supposed two-body projectile was given in equation (2) with $U(\vec{r},\vec{R}) = V_{vt} + V_{ct}$ the total interaction between the projectile and target. These interactions are calculated assuming $j = c, v$ have energies $E_j = m_j E/M$ with $M = m_c + m_v$ the projectile mass. Since the projectile is assumed to have only one bound state ϕ_0, all excited states of H_p, $\phi_{\vec{k}}$, are positive energy scattering states in the continuum with energy ε_k.

The projectile will be excited (dissociated) or coupled to these excited states through the interaction $U(\vec{r},\vec{R})$, since the resulting tidal forces $\vec{F}_j = -\nabla V_{jt}(\vec{r}_j)$ are different on the two (or more) individual constituents. These bound state to continuum state couplings are $\langle\phi_{\vec{k}}|U(\vec{r},\vec{R})|\phi_0\rangle$ and the range of energies of the $\phi_{\vec{k}}$ states which are strongly excited will be dictated by the geometries of the potentials V_{jt}. When the target nucleus is heavy and of large Z, and Coulomb dissociation is dominant, then the slow spatial rate of change of the Coulomb interaction leads to weak tidal forces and strong excitation of the low energy continuum. An excellent example of such a situation is the experimental study of the Coulomb dominated ^{19}C breakup by a Pb target at 67 MeV/nucleon by Nakamura et al. [13]. In that case the cross section for breakup is dominated by breakup energies $\varepsilon_k \leq 3$ MeV. In other words the Coulomb interactions with the target are able to transfer very little of the incident energy of the projectile into excitation energy as relative kinetic energy between the projectile constituents.

In the case of light nuclear targets where the strong interaction dominates, the sharper (less diffuse) surface potential leads to larger and more surface localised tidal forces with a greater range of ε_k excited. Nevertheless, the surface diffuseness of nuclear potentials has a rather universal value, of order 0.6 fm, and so the differential forces are themselves rather universal in

strength. The typical maximum breakup excitation energies, for projectiles on a light target, are found to be of order 20 MeV, and essentially independent of the incident projectile energy [14, 15, 16]. Are these excitation energies important?

The answer is yes. It is important for what follows that these excited breakup configurations have typical internal energies $\langle H_p \rangle \ll E$, the energy of the projectile centre of mass motion. It follows that the velocities of relative motion of c and v are slow. In this case where one degree of freedom (motion) is slow and another is fast, we can make a major simplification to the description of the reaction dynamics - the adiabatic approximation.

4.1. THE ADIABATIC APPROXIMATION

The adiabatic (or sudden) approximation is used widely throughout physics when one can identify certain degree(s) of freedom in a problem as being highly energetic, or *fast*, and another as being of low energy, or *slow*. In such cases it may be appropriate to fix or freeze the slow coordinate (degree of freedom) for the duration of the fast passage or interaction in the other degree of freedom. Examples are the scattering of fast particles from a deformed rotor (with orientation $\hat{\Omega}$) or from a diatomic vibrational molecule (with separation $\vec{R}$). In the former case, the calculation proceeds by calculating the scattering amplitude $f(\theta, \hat{\Omega})$ at each fixed $\hat{\Omega}$. Of course in freezing the orientation, formally one is assuming that that moment of inertia of the rotor is infinite and hence that the full rotational excitation spectrum of the rotor is degenerate with the ground state. The $f(\theta, \hat{\Omega})$ thus represent scattering from a degenerate superposition of all states of the rotor and the physical amplitudes for given initial and final states $|\alpha\rangle$ and $|\beta\rangle$ are obtained by projection, i.e. $f_{\alpha\beta}(\theta) = \langle\beta|f(\theta, \hat{\Omega})|\alpha\rangle$. The beauty of such an approach is that it separates the scattering dynamics, in $f(\theta, \hat{\Omega})$, from the structural aspects of the problem, in states $|\alpha\rangle$ and $|\beta\rangle$.

In the nuclear few-body (reaction) context the slow coordinate is the cv relative motion, $\vec{r}$, which we assume frozen for the duration of the collision of the projectile with the light nuclear target. Thus, at each fixed $\vec{r}$, we must calculate a scattering amplitude $f(\theta, \vec{r})$, describing scattering of a superposition of the projectile ground and all excited states, assumed degenerate. As previously, physical amplitudes are obtained by suitable overlaps being taken, the breakup amplitude to final state $\phi_{\vec{k}}$ being $f_{\vec{k}}(\theta) = \langle\phi_{\vec{k}}|f(\theta, \vec{r})|\phi_0\rangle$. The bra-ket indicates integration over all position vectors $\vec{r}$. Given the limited range of ε_k excited in the scattering, the adiabatic approximation will improve systematically with increasing incident energy.

For practical purposes, the degeneracy assumed in the adiabatic assumption is included in the few-body Schrödinger equation by replacing

$H_p \rightarrow -\varepsilon_0$, the projectile's ground state energy eigenvalue, to give the corresponding adiabatic model Schrödinger equation

$$\left[T_R + U(\vec{r},\vec{R}) - (E+\varepsilon_0) \right] \Psi^{Ad}_{\vec{K}}(\vec{r},\vec{R}) = 0 \quad . \tag{11}$$

The adiabatic approximation has been applied extensively in few- body physics [17, 18, 19, 20, 21, 22, 23].

4.2. FEW-BODY EIKONAL MODEL

The solution of the adiabatic few-body equation is particularly informative in the eikonal approximation. The derivation follows closely that used for a point particle in Section 3.2. As there, the scattering wave function is written as the product of the incident wave with a modulating function. This now reads

$$\Psi^{Ad}_{\vec{K}}(\vec{r},\vec{R}) = e^{i\vec{K}\cdot\vec{R}}\,\phi_0(\vec{r})\omega(\vec{r},\vec{R}) \ , \tag{12}$$

with $\hbar K = \sqrt{2\mu(E+\varepsilon_0)}$. Upon substituting in the adiabatic Schrödinger equation (11), then

$$\left[2i\nabla_R\omega(\vec{r},\vec{R})\cdot\vec{K} - \frac{2\mu}{\hbar^2}U(\vec{r},\vec{R})\omega(\vec{r},\vec{R}) + \nabla^2_R\omega(\vec{r},\vec{R}) \right] \exp(i\vec{K}\cdot\vec{R}) = 0 \ , \tag{13}$$

and neglecting the curvature term, $\nabla^2_R\omega$, yields the solution for ω of

$$\omega(\vec{r},\vec{R}) = \exp\left\{ -\frac{i}{\hbar v}\int_{-\infty}^{Z} U(\vec{r},\vec{R}')dZ' \right\} \quad . \tag{14}$$

As $U(\vec{r},\vec{R})$ is the sum of the constituent two-body interactions V_{jt} with the target, it follows that asymptotically ($Z \rightarrow \infty$), after the interaction, the eikonal approximation to the few-body wave function is

$$\Psi^{Eik}_{\vec{K}}(\vec{r},\vec{R}) \rightarrow S_c(b_c)S_v(b_v)e^{i\vec{K}\cdot\vec{R}}\,\phi_0(\vec{r}) \ , \tag{15}$$

where, as in equation (10), the $S_j(b_j)$ are the eikonal elastic S-matrices for the independent scattering of particle j from the target, when incident with velocity v.

In the spirit of the adiabatic approximation, $\vec{r}$ enters this approximate wave function only as a parameter, and the expression calculates the S-matrices for a frozen cv separation, and hence fixed b_c, b_v, and b, the impact parameter of the centre of mass of the projectile. It follows that the probability amplitude for the projectile surviving the collision and emerging in its ground state, the elastic S-matrix for the projectile, $S_p(b)$, at c.m. impact parameter b is

$$S_p(b) = \langle\phi_0|S_c(b_c)S_v(b_v)|\phi_0\rangle \ . \tag{16}$$

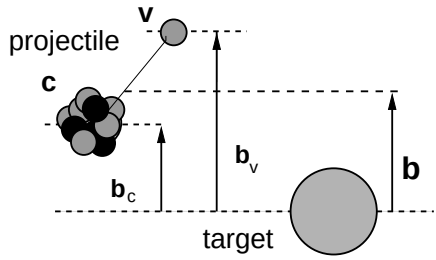

Figure 3. Frozen internal coordinates and straight line trajectories are assumed in the few-body eikonal approximation

From a reaction theory and spectroscopic point of view equation (16) is particularly transparent since it separates formally the dynamical aspects (the S_j), determined by independent two particle scattering theory/experiment, from the structural aspect, the wave function of the projectile which we want to probe. This matrix element includes (within the adiabatic and eikonal approximations) the breakup of the projectile by the tidal forces induced by the target to all orders and is a non-perturbative theory of the reaction.

The formulae presented generalise in an obvious way to projectiles with n constituents, and for excitation of a final state α, with a general structure,

$$S_\alpha(b) = \langle \Phi_\alpha | S_1(b_1) S_2(b_2) \dots S_n(b_n) | \Phi_0 \rangle \ . \tag{17}$$

For RIBs from fragmentation reactions, with energies of order 50 MeV per nucleon and greater, this few-body eikonal picture as been shown to be rather accurate [24, 25, 26, 27, 28, 29, 30, 31, 32, 33, 34, 35, 36] and so forms a viable scheme from which to interpret experimental data. The clear formal separation of the structure and dynamical inputs allows the best available few- or many-body wave functions to be used in computing S_p. Recent examples include the use of a 5-body (α+4 neutron) wave function for ^{8}He scattering [29] and of fully microscopic 6-body QMC wave functions for ^{6}Li and ^{6}He to describe their scattering from a proton target [37].

The Sections above have put the different reaction theory approximations in place, including the non-perturbative treatment of breakup which is crucial in the case of weakly bound systems.

5. Few-body reaction observables

As was discussed in the Introduction, for single particle spectroscopy we wish, if possible, to excite the projectile minimally, ideally involving affecting the degrees of freedom of a single nucleon. In the following we use this

formalism for calculations of single-nucleon knockout reactions. We emphasise however that the expressions we will write down are only valid at high beam energies and low excitation energies since detailed energy conservation is not respected in the adiabatic and eikonal models.

Returning to our two-body $(c+v)$ projectile, the total cross section for populating a given final state α is

$$\sigma_\alpha = \int d\vec{b}\, |\langle\phi_\alpha|S_c(b_c)S_v(b_v)|\phi_0\rangle - \delta_{\alpha 0}|^2 \ . \tag{18}$$

When $\alpha = 0$, the total elastic cross section is

$$\sigma_{el} = \int d\vec{b}\, |1 - \langle\phi_0|S_c(b_c)S_v(b_v)|\phi_0\rangle|^2. \tag{19}$$

The total cross section is also obtained from the elastic scattering amplitude, employing the optical theorem, and gives

$$\sigma_{tot} = 2\int d\vec{b}\,[1 - \mathcal{R}e\,\langle\phi_0|S_c(b_c)S_v(b_v)|\phi_0\rangle]\,. \tag{20}$$

Hence, the total reaction cross section, defined as the difference between these total and elastic cross sections, is

$$\sigma_R = \int d\vec{b}\left[1 - |\langle\phi_0|S_c(b_c)S_v(b_v)|\phi_0\rangle|^2\right]. \tag{21}$$

As we have noted, for projectiles with only one bound state, any excitation will be to the continuum with wave function $\phi_{\vec{k}}$. This process, the target remaining in its ground state, is elastic breakup, also referred to as diffractive dissociation. Making use of the completeness relation for states of H_p (when, for simplicity, there is only one bound state)

$$\int d\vec{k}\ |\phi_{\vec{k}}\rangle\langle\phi_{\vec{k}}| = 1 - |\phi_0\rangle\langle\phi_0| \tag{22}$$

the total elastic (diffractive) breakup cross section is

$$\sigma_{diff} = \int d\vec{b}\left[\langle\phi_0|\ |S_c(b_c)S_v(b_v)|^2|\phi_0\rangle - |\langle\phi_0|S_c(b_c)S_v(b_v)|\phi_0\rangle|^2\right]\ . \tag{23}$$

The difference between the reaction and elastic breakup cross section is therefore the total absorption cross section,

$$\sigma_{abs} = \int d\vec{b}\left[1 - \langle\phi_0|\ |S_c(b_c)S_v(b_v)|^2|\phi_0\rangle\right]\ , \tag{24}$$

which represents the cross section for excitation of the target.

The physical meaning of the above is understood by a reminder that the square modulus of each constituent's S-matrix element, $|S_j(b_j)|^2$ represents the probability that it survives intact with the target in its ground state following interaction with the target at impact parameter $\vec{b}_j$. That is, at most, it is elastically scattered. At large impact parameters $|S_j|^2 \to 1$ since the constituent passes too far from the target. The quantity $1 - |S_j|^2$ is the probability that particle j interacts with and excites the target and is absorbed from the elastic channel. With this picture in mind and noting that the integrand in equation (24) can be written

$$1-|S_cS_v|^2 = |S_v|^2(1-|S_c|^2)+|S_c|^2(1-|S_v|^2)+(1-|S_v|^2)(1-|S_c|^2), \quad (25)$$

that part of the absorption cross section for stripping v from the projectile, exciting the target, but with c surviving (having been at most elastically scattered) is

$$\sigma_{str} = \int d\vec{b}\ \langle\phi_0||S_c(b_c)|^2[1-|S_v(b_v)|^2]|\phi_0\rangle. \quad (26)$$

This cross section is seen to vanish if the interaction V_{vt} with the target is real and non-absorptive, and hence $|S_v(b_v)| = 1$. Related expressions for the differential stripping cross sections as a function of the final momentum of the core fragment can also be found in the bibliography, eg. [27].

6. Single-nucleon knockout reactions

In nucleon knockout reactions, events in which a single nucleon (the valence particle v) is removed from the mass A projectile nucleus p by a light absorptive nuclear target (typically ^{9}Be or ^{12}C) are identified by detection of the core nuclei c, of mass $A-1$.

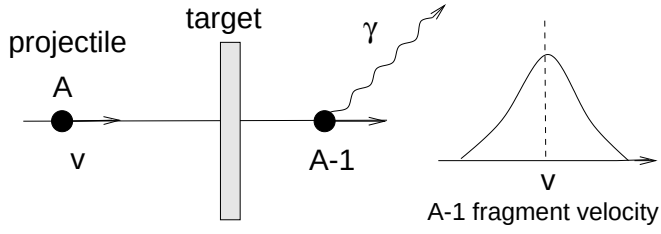

Figure 4. Schematic of a single nucleon knockout reaction, where the momentum distribution of the mass $A-1$ fragment and in-flight decay photons are obtained.

The detected residues travel with a velocity very close to that of the incident beam. Since only the heavy residue c is detected and not the removed nucleon or state of the target, the measurement is a highly inclusive

one and the cross sections are thus expected to be large. This is extremely advantageous from an experimental point of view.

The use of a light nuclear target introduces spatial localisation of the reaction at the nuclear surface. ^{9}Be in particular, having no bound excited states, essentially presents a black absorptive disk to the incident core of nucleons c. The fact that in the events observed c survives at near to beam velocity, dictates that the ct interactions are extremely peripheral. It follows that the removed nucleon's wave function will be probed at and beyond the surface of the projectile, but not in the interior. This is a very similar situation to that in low-energy light-ion induced transfer reactions where the short mean-free-paths of the light-ions with the target also leads to strong surface localisation [2].

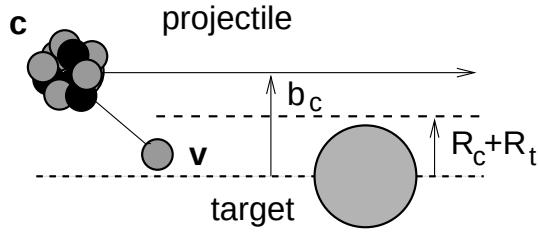

Figure 5. The requirement that the core fragment survives the collision dictates that the reaction is peripheral (that $b_c \geq R_c + R_t$) and hence that only that part of the valence particle wave function outside of the core is sampled (and $b_v \leq R_c + R_t$).

The cross sections are the sum of (a) those for all processes in which the removed nucleon excites the target and is absorbed, called stripping above, and given by equation (26), and (b) the cross section for elastic breakup of the projectile, the target remaining in its ground state, called diffractive dissociation above and given by equation (23). These cross sections can simply be added since the two processes lead to quite distinct final states and are thus incoherent, so

$$\sigma(c) = \sum C^2 S(c, \ell j) \sigma_{sp}(S_n, \ell j). \tag{27}$$

Here C^2S is the spectroscopic factor (occupancy) of the nucleon's single-particle state with quantum numbers (ℓj), and expresses the parentage of this single-particle configuration in the initial many-body wave function Φ_A with respect to a specific core state c of the remaining nucleons. The sum must be taken over all non-vanishing configurations. The σ_{sp} are the cross sections for the removal of a single particle, from the stripping and diffraction mechanisms, ie. $\sigma_{sp} = \sigma_{str} + \sigma_{diff}$, for a nucleon with separation energy S_n.

The important development, for spectroscopy, are measurements, not only of the momentum of c, but also its final state ϕ_c, by detection in coincidence with in-flight decay photons. Even in the most naive extreme single-particle shell model picture, see Figure 6, it is clear that removal of other than the least bound nucleon will leave c in an excited configuration. The decay photon is able to tag this information and to identify the final state of c which is populated.

6.1. AN EXAMPLE: FOR ORIENTATION

We consider for orientation the example in Figure 6, neutron removal from ^{23}O in an extreme single-particle model. A recent experiment at RIKEN, on a ^{12}C target at 72 MeV per nucleon [38], and without γ-detection, measures a cross section of 233(37) mb for the production of ^{22}O.

We assume that the neutron configuration of ^{23}O(gs) is $[1s_{1/2}][0d_{5/2}]^6$. The ground state to ground state neutron separation energy is 2.7 MeV and the shell model predicts a $5/2^+$ state in ^{22}O at 2.75 MeV. Thus we assume a $0d_{5/2}$ neutron separation energy of 5.5 MeV. The remaining 8 neutrons are very strongly bound and so contribute very small cross sections for knockout. In this simple model, equations (26) and (23), with S-matrices calculated according to [39], calculate sp cross sections $\sigma_{sp}(1/2^+) = 64$ mb and $\sigma_{sp}(5/2^+) = 23$ mb. Upon multiplying by the spectroscopic factors of 1 and 6, respectively, this gives a predicted theoretical cross section of 202 mb in good agreement with the measurement. Moreover, the prediction is that less than one third of the cross section (64 mb) is attributable to the ^{22}O being formed in its ground state and the expectation is that two-thirds of the cross section (138 mb) would leave ^{22}O in the $5/2^+$ excited state and which will be accompanied by a decay photon.

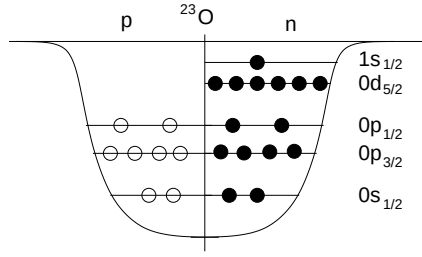

Figure 6. A simple extreme single-particle shell model representation for the ^{23}O(gs). Removal of different nucleons will leave the residue in the ground or an excited state configuration for ^{22}O.

This simple example shows that the cross sections for producing core

fragments in excited states are expected to be very significant, even for halo nuclei with a very weakly bound valence nucleon moving relative to the ground state of c as a dominant configuration. The non-halo nucleons are more bound but are also more numerous, i.e. have larger C^2S. So, extracting quantitative spectroscopic information of even the dominant configurations in the many-body projectile wave function from measurements that do not identify the final state of c, e.g. [40], is very difficult, given these large cross sections from the removal of more-bound nucleons. With c state exclusive measurements, the reaction theory introduced above, together with structure theory, can be used to interpret the different c state momentum distributions and cross sections in terms of the removed nucleon's state ϕ_0 – specifically, the orbital angular momentum ℓ and spectroscopic factor C^2S of this configuration. The orbital angular momentum ℓ of the knocked-out nucleon is identified uniquely by the widths of the measured momentum distributions of the residues, as is shown in the models in Refs. [25, 26]. Since the C^2S multiply the sp cross sections they are determined 'experimentally' by comparing the magnitudes of the measured partial cross sections to each final state of c with the σ_{sp} calculated using the eikonal reaction theory.

6.2. STRUCTURE OVERLAP FUNCTIONS

Inherent in analyses of both knockout reaction and transfer reaction data is the need to learn the extent to which the intensities of the core states ϕ_c, measured following the reaction, reflect a pre-existing component in the incident projectile wave function Φ_A. Alternatively, how important are those (higher-order) dynamical processes which could result in the outgoing flux being redistributed between core states by the reaction dynamics.

Here it was already assumed in the orienting example above that there are pre-formed components in the ground state wave function of the incident A-body projectile in which $A-1$ of the nucleons are in state ϕ_c, and which can therefore be accessed by a single-nucleon knockout. Explicit inelastic excitation of the state of these $A-1$ nucleons is absent in the reaction mechanism and is neglected in any final state interactions of the core with the target or with the removed nucleon. It follows that the reaction mechanism then reduces to an effective three-body (nucleon+c+target) problem in which the core is simply a spectator particle which can therefore interact at most elastically with the target. This is the basis of the formalism presented and is expected to be a good starting point for low lying states of the projectile with strong core state parentage. In common with other spectroscopic methods, for weakly populated ϕ_c configurations, and core states with only small parentage in the projectile ground state,

higher order dynamical effects may be significant.

In the spectator core picture [41], quite generally, the structure inputs to the three-body reaction formalism are the single nucleon formfactors or overlaps

$$F^c_{\ell j}(\vec{r}) = \langle \phi_c, \vec{r} | \Phi_A \rangle \quad . \tag{28}$$

Formally the spectroscopic factor, normalised to the occupancy of the given state, is

$$C^2S(c, \ell j) = \int d\vec{r} |F^c_{\ell j}(\vec{r})|^2 \ . \tag{29}$$

It is usual however to rewrite the overlap formfactor as

$$F^c_{\ell j}(\vec{r}) = [C^2S(c, \ell j)]^{1/2} \phi_{\ell j}(\vec{r}) \ , \tag{30}$$

where the single particle state $\phi_{\ell j}$, normalised to unity, is used for ϕ_0 in equations (26) and (23). The spectroscopic factor can be taken from structure calculations, such as configuration mixed psd-shell model calculations. Similarly, if they were generally available, theoretical many-body overlap functions could be taken for $\phi_{\ell j}$. In practice these are not routinely available and the practice, as in transfer reactions, is to calculate the $\phi_{\ell j}$ as single particle wave functions in a Woods-Saxon potential well of conventional geometry (radius $r_0 = 1.25$ fm and diffuseness $a_0 = 0.65$ fm) and with the physical separation energy for each pair of states ϕ_c and Φ_A. This provides the input needed to systematically investigate available experimental data for a wide variety of systems.

The techniques outlined here have recently been applied in a number of important spectroscopic cases including the phosphorus isotopes ^{26,27,28}P [42], ^{11,12}Be [43, 44, 45], ^{13,14}B [46], ^{34,35}Si and ^{37}S [47], ^{8}B [48, 49] and the neutron-rich carbon isotopes ^{15,16,17,19}C [39]. The reader is referred to these publications for further details of the experimental arrangements and theoretical inputs. These analyses have also recently been reviewed by Hansen and Sherrill [50]. Here we illustrate the method and data with a few selected examples which bring out several interesting and important results.

6.3. PROTON HALOS IN THE PHOSPHORUS ISOTOPES?

The first application of the nucleon knockout reaction with photon coincidences was an exploratory experiment, at the NSCL, for the ^{26,27,28}P isotopes. Here the expectation from shell model calculations is that the ^{28}P ground state has a weakly bound $1s_{1/2}$ proton (separation energy 2.07 MeV) outside of a ^{27}Si($5/2^+$) ground state core – and that ^{26}P is a proton halo nucleus candidate. Figure 7 is taken from Ref. [42] and shows, in the

lower part (b), the momentum distributions of the ^{27}Si residues measured without (solid points) and with (open points) a γ ray in coincidence. The data are for the proton removal from a ^{28}P beam on a ^{9}Be target at 65 MeV per nucleon.

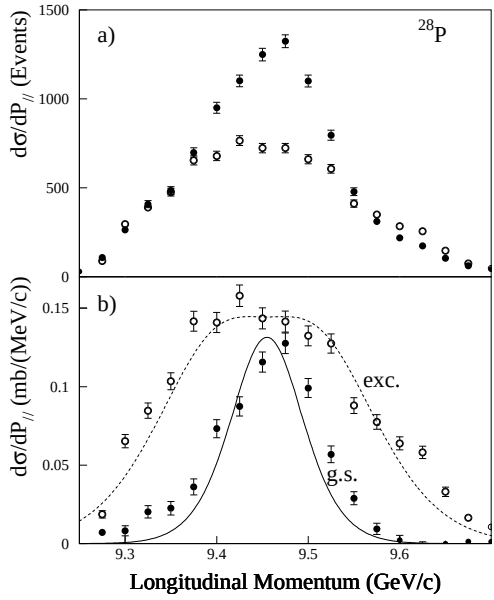

Figure 7. Parallel momentum distributions of ^{27}Si residues, following proton knockout from a ^{28}P beam at 65 MeV/nucleon, from [42], measured with (open points) and without (solid points) a photon in coincidence.

The curves show the theoretical distributions expected on the basis of removal of an *s*-state (solid curve) and *d*-state (dashed curve) proton of the appropriate separation energy. In this experiment the different excited state contributions were not well resolved and are summed in the excited state distribution. The data show the expected ℓ assignments unambiguously and the measured integrated cross sections for the three isotopes are consistent with the reaction theory and shell model spectroscopic factors.

6.4. NEUTRON REMOVAL FROM ^{17}C

The level of information which can be gained from nucleon knockout, in coincidence with gamma ray detection, is illustrated by the analysis of neutron removal from ^{17}C, and shown in Fig. 8.

Here the momentum distribution of the ^{16}C residues are shown which correspond to the ground state, the first 2^+ state and the (unresolved) set

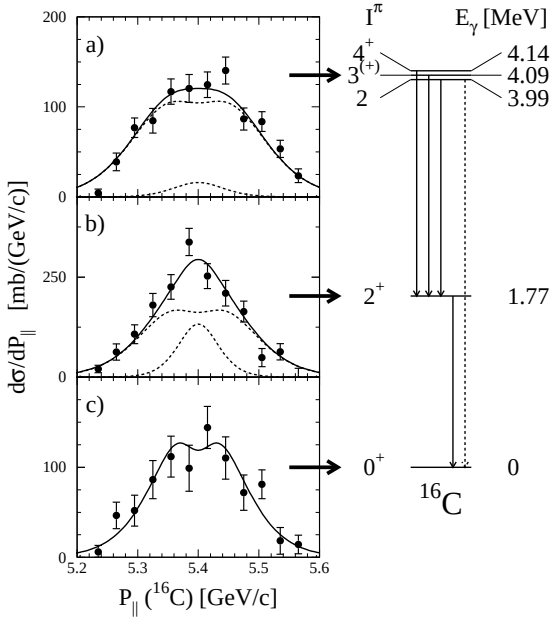

Figure 8. Parallel momentum distributions of ^{16}C residues, following neutron knockout from a ^{17}C beam on a ^{9}Be target at 60 MeV/nucleon, from [39].

of states at 4 MeV of excitation of ^{16}C. The data for these three final states are shown in parts (a), (b) and (c) of the figure, respectively.

The curves are the result of the theoretical, eikonal model calculations [39]. They reveal the expected $\ell = 2$ nature of the ground state to ground state transition while the momentum distribution of residues for the 2^+ transition indicates an admixture of $\ell = 0$ and 2 configurations with magnitudes in good agreement with shell model expectations. Similarly the distribution of residues populated in the three 4 MeV excited states shows a dominant $\ell = 2$ removal process, consistent with structure calculations.

6.5. THE $N = 8$ NEUTRON SHELL CLOSURE IN ^{12}BE

A very interesting and important example is the neutron removal reaction from ^{12}Be. Experimental information on the ^{11}Be(gs) from different sources is now broadly in agreement. An inverse kinematics ^{11}Be(p,d) experiment at GANIL [3] gives results consistent with an s-wave–^{10}Be(0^+) component in excess of 70% and a 10–20% d-wave–^{10}Be(2^+) neutron component in the ^{11}Be(gs). Theoretical predictions from shell model calculations [44], are in agreement with this, and with the findings of the ^{9}Be(^{11}Be,^{10}Beγ) one-neutron knockout experiment performed at the NSCL [46]. Since the

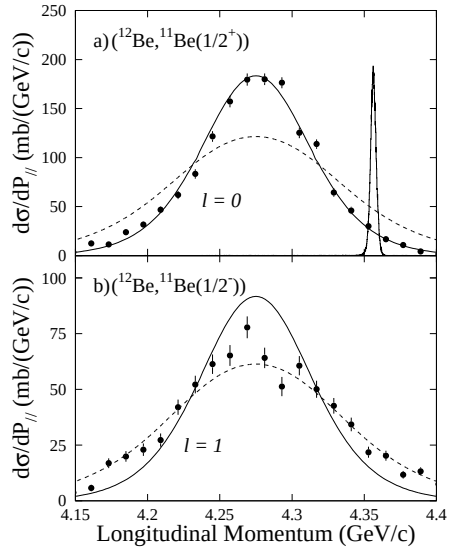

Figure 9. Parallel momentum distributions of ^{11}Be residues, following neutron knockout from a ^{12}Be beam on a ^{9}Be target at 78 MeV/nucleon, from [44], measured with (lower graph) and without (upper graph) the ^{11}Be$(1/2^-)$ state decay photon in coincidence.

valence neutron in the ^{11}Be(gs) occupies the sd-shell, an important question is whether one recovers the $[0p_{1/2}]^2$ closed shell configuration in ^{12}Be upon addition of a neutron. This is of interest not only for the structure of ^{12}Be but also for that of the heavier beryllium isotopes.

If the $[0p_{1/2}]^2$ closed shell configuration is indeed restored in ^{12}Be then neutron removal will populate preferentially the ^{11}Be$(1/2^-)$ excited state, and a decay photon will be observed. If on the other hand the last two neutrons occupy the sd-shell, neutron knockout will preferentially feed the ^{11}Be(gs).

This experiment was carried out at the NSCL [44]. Figure 9 shows the cross section momentum distributions to the ^{11}Be(gs) (upper) and ^{11}Be$(1/2^-)$ excited state (lower), which are found to be populated with almost equal strength. The measured and calculated momentum distributions confirm the $\ell = 0$ and $\ell = 1$ nature of these two transitions. In addition the deduced spectroscopic factors for these transitions indicate there is missing experimental cross section which is expected to reside in the $[0d_{5/2}]^2$ configuration. The latter was not seen in this experiment as the neutron removal from this component will populate the ^{11}Be$(5/2^+)$ state in the continuum leading to a mass 10 residue. This analysis reveals very clearly the melting of the $N = 8$ magic number in ^{12}Be and the complexity of the ^{12}Be(gs) wave function.

6.6. SUMMARY: EIKONAL KNOCKOUT THEORY

In this Section we have provided an introduction, together with examples selected from recent analyses, of the ideas behind the application of the approximate adiabatic plus eikonal few-body reaction approach to single-nucleon knockout reactions. References to a wider range of recent studies were given earlier. The extent to which the spectroscopic factors C^2S(Experiment), deduced from the measured $\sigma(c)$ and the theoretical $\sigma_{sp}(c, \ell j)$ using equation (27), agree with those of multi-configuration shell model calculations, C^2S(Theory), are presented in Fig. 10 for all cases currently available. The agreement is very promising, with good overall agreement over the range of nuclei studied to date. This work is ongoing.

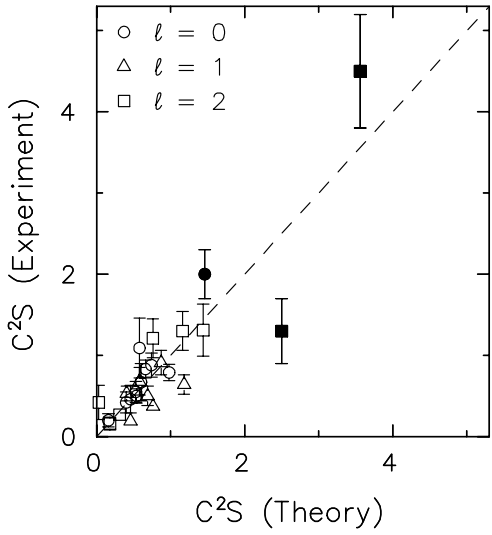

Figure 10. Experimentally deduced C^2S values (fitted to data for individual transitions), on the vertical axis, versus theoretical C^2S values calculated from the shell model, on the horizontal axis. The figure is from [47]. Calculations and measurements cover a number of transitions and projectile nuclei. The agreement is within the experimental error bars in essentially all cases.

Effort is now being given to a far more rigorous assessment of the accuracy of the approximate scheme described. This involves comparisons with the results from data taken at higher energies, where the adiabatic and eikonal approximations are very accurate, and studies of improved fully quantum mechanical dynamical reaction models at energies such as are considered here. See for example [16]. The conclusion of the work of Ref. [16] is that the errors in the approximate treatment are actually rather small and affect details of the shapes of the calculated momentum distributions, but

not the overall magnitudes of the cross sections, which are most important for spectroscopy. The long term objective is to ascertain how reliably and quantitatively the knockout reaction approach can extract absolute values of the C^2S, or occupancies, of single particle states in exotic nuclei. The possibility to investigate the additional effects of short range correlations in nuclei is also being considered [48].

7. Concluding remarks

Due to the severe time constraints of these lectures I have been deliberately very selective in my choice of material. I wanted to show how, by suitable choices of approximation schemes, one is able to make progress from the effective few-body Hamiltonian for the original interacting system to rather simple expressions for the elastic and inelastic S-matrices of the projectile-target system and thence to relatively simple expressions for reaction observables. These expressions were then compared with experimental data and, I hope, this approach has made the motivation for the approximation schemes more tangible. Moreover, they appear to offer an effective and simple approach to single-nucleon spectroscopy of rare exotic nuclei.

Of course these approximate calculations, or elements thereof, must be tested using more accurate theories, where these are available, but there was insufficient time for these alternative approaches to be discussed here. The best non-adiabatic and non-eikonal few-body reaction models available are based on coupled channels [14, 15, 51, 52, 53, 54, 55, 16, 56] and time-dependent [57, 58, 59] formulations and methods. Systematic improvements of the adiabatic and eikonal approximations are also being studied, e.g. [34, 23] and references therein. All of these methods permit comparisons and testing of different aspects of the approximations used here. The reader is referred to these papers, and the numerous references therein, for details of these methods and their ranges of applicability.

References

1. G.J. Kramer, H.P. Blok and L.Lapikas, *Nucl. Phys. A* **679**, 267.
2. N.K. Glendenning, One- and two-nucleon transfer reactions, *Chapter IX.E, in Nuclear Spectroscopy and Reactions, Vol. D, ed J. Cerny, Academic Press*, 319.
3. J. Winfield et al., Single-neutron transfer from ^{11}Be(gs) via the (p,d) reaction with a radioactive beam, *Nucl. Phys. A* **683**, 48.
4. N. K. Timofeyuk and R. C. Johnson, Deuteron stripping and pick-up on halo nuclei, *Phys. Rev. C* **59**, 1545.
5. F. M. Nunes and A. M. Mukhamedzhanov, Are coupled channel effects important for the asymptotic normalization coefficient method?, *Phys. Rev. C* **64**, 062801.
6. Yu. Ts. Oganessian, V. I. Zagrebaev, and J. S. Vaagen, Dynamics of two-neutron transfer reactions with the Borromean nucleus ^{6}He, *Phys. Rev. C* **60**, 044605.

7. N. Austern, *Direct Nuclear Reaction Theories*, New York: Wiley (1970).
8. G.R. Satchler, *Direct Nuclear Reactions*, Oxford: Clarendon Press (1983).
9. J.S. Al-Khalili and J.A. Tostevin, Matter radii of light halo nuclei, *Phys. Rev. Lett.* **76**, 3903.
10. J.S. Al-Khalili, J.A. Tostevin and I.J. Thompson, Radii of halo nuclei from cross section measurements, *Phys. Rev. C* **54**, 1843.
11. R.J. Glauber, *High-energy Collision theory*, In W.E. Brittin (ed) *Lectures in Theoretical Physics*, Vo1. 1: 315. New York: Interscience (1959).
12. R.G. Newton, *Scattering theory of waves and particles*, New York: McGraw-Hill (1966).
13. T. Nakamura et al., *Phys. Rev. Lett.* **83**, 1112.
14. M. Kamimura, M. Yahiro, Y. Iseri, Y. Sakuragi, H. Kameyama, and M. Kawai, Coupled-channels theory of breakup processes in nuclear reactions, *Prog. Theor. Phys. Supplement* **89**, 1.
15. N. Austern, Y. Iseri, M. Kamimura, M. Kawai, G. Rawitscher and M. Yahiro, Continuum discretized coupled-channels calculations for three-body models of deuteron-nucleus reactions, *Phys. Rep.* **154**, 125.
16. J. A. Tostevin, D. Bazin, B. A. Brown, T. Glasmacher, P. G. Hansen, V. Maddalena, A. Navin, and B. M. Sherrill, Single-neutron removal reactions from ^{15}C and ^{11}Be: Deviations from the eikonal approximation, *Phys. Rev. C* **66**, 024607.
17. J.A. Christley, J.S. Al-Khalili, J.A. Tostevin and R.C. Johnson, Four-body adiabatic model applied to elastic scattering, *Nucl. Phys. A* **624**, 275.
18. R. C. Johnson, J. S. Al-Khalili, and J.A. Tostevin, Elastic Scattering of Halo Nuclei, *Phys. Rev. Lett.* **79**, 2771.
19. J.A. Tostevin et al., Coulomb breakup of light composite nuclei, *Phys. Lett. B* **424**, 219.
20. J. A. Tostevin, S. Rugmai, and R. C. Johnson, Coulomb dissociation of light nuclei, *Phys. Rev. C* **57**, 3225.
21. P. Banerjee, J. A. Tostevin, and I. J. Thompson, Coulomb breakup of two-neutron halo nuclei, *Phys. Rev. C* **58**, 1337.
22. R.C. Johnson, Scattering and reactions of halo nuclei, *Prog. Theor. Phys. Supplement* **140**, 33.
23. N. C. Summers, J. S. Al-Khalili, and R. C. Johnson, Nonadiabatic corrections to elastic scattering of halo nuclei, *Phys. Rev. C* **66**, 014614.
24. J.S. Al-Khalili, I.J. Thompson and J.A. Tostevin, Evaluation of an eikonal model for ^{11}Li-nucleus elastic scattering, *Nucl. Phys. A* **581**, 331.
25. P. G. Hansen, Momentum Content of Single-Nucleon Halos, *Phys. Rev. Lett.* **77** 1016.
26. H. Esbensen, Momentum distributions in stripping reactions of single-nucleon halo nuclei, *Phys. Rev. C* **53**, 2007.
27. K. Hencken, G. Bertsch, and H. Esbensen, Breakup reactions of the halo nuclei ^{11}Be and ^{8}B, *Phys. Rev. C* **54**, 3043.
28. J.A. Tostevin and J.S. Al-Khalili, How large are the halos of light nuclei?, *Nucl. Phys. A* **616**, 418.
29. J. A. Tostevin, J. S. Al-Khalili, M. Zahar, M. Belbot, J. J. Kolata, K. Lamkin, D. J. Morrissey, B. M. Sherrill, M. Lewitowicz, and A. H. Wuosmaa, Elastic and quasielastic scattering of ^{8}He from ^{12}C, *Phys. Rev. C* **56**, R2929.
30. J. S. Al-Khalili and J. A. Tostevin, Few-body calculations of proton- ^{6,8}He scattering, *Phys. Rev. C* **57**, 1846.
31. G. F. Bertsch, K. Hencken, and H. Esbensen, Nuclear breakup of Borromean nuclei, *Phys. Rev. C* **57**, 1366.
32. H. Esbensen and G. F. Bertsch, Nuclear induced breakup of halo nuclei, *Phys. Rev. C* **59**, 3240.
33. Henning Esbensen and Kai Hencken, Systematic study of ^{8}B breakup cross sections, *Phys. Rev. C* **61**, 054606.

34. J. M. Brooke, J. S. Al-Khalili, and J. A. Tostevin, Noneikonal calculations for few-body projectiles, *Phys. Rev. C* **59**, 1560.
35. J. A. Tostevin and J. S. Al-Khalili, Calculations of reaction cross sections for ^{19}C at relativistic energies, *Phys. Rev. C* **59**, R5.
36. J.A. Tostevin, R.C. Johnson and J.S. Al-Khalili, Manifestation of halo size in scattering and reactions, *Nucl. Phys. A* **630**, 340.
37. K. Varga et al., ANL Preprint 2002.
38. R. Kanungo et al., *Phys. Rev. Lett.* **88**, 142502.
39. V. Maddalena, T. Aumann, D. Bazin et al., Single-neutron knockout reactions: Application to the spectroscopy of ^{16,17,19}C, *Phys. Rev. C* **63**, 024613.
40. E. Sauvan et al., One-neutron removal reactions on neutron-rich psd-shell nuclei, *Phys. Lett. B* **491**, 1.
41. J.A. Tostevin, Single-nucleon knockout reactions at fragmentation beam energies, *Nucl. Phys. A* **682**, 320.
42. A. Navin, et al., Spectroscopy of Radioactive Beams from Single-Nucleon Knockout Reactions: Application to the sd Shell Nuclei ^{25}Al and ^{26,27,28}P, *Phys. Rev. Lett.* **81**, 5089.
43. J.A. Tostevin, Core excitation in halo nucleus breakup, *J. Phys. G: Nucl. Part. Phys.* **25**, 735.
44. A. Navin, et al., Direct Evidence for the Breakdown of the N = 8 Shell Closure in ^{12}Be, *Phys. Rev. Lett.* **85**, 266.
45. T. Aumann, et al., One-Neutron Knockout from Individual Single-Particle States of ^{11}Be, *Phys. Rev. Lett.* **84**, 35.
46. V. Guimares, J. J. Kolata, D. Bazin, B. Blank, B. A. Brown, T. Glasmacher, P. G. Hansen, R. W. Ibbotson, D. Karnes, V. Maddalena, A. Navin, B. Pritychenko, B. M. Sherrill, D. P. Balamuth, and J. E. Bush, Spectroscopy of ^{13,14}B via the one-neutron knockout reaction, *Phys. Rev. C* **61**, 064609.
47. J. Enders, A. Bauer, D. Bazin et al., Single-neutron knockout from ^{34,35}Si and ^{37}S, *Phys. Rev. C* **65**, 034318.
48. B. A. Brown, P. G. Hansen, B. M. Sherrill et al., Absolute spectroscopic factors from nuclear knockout reactions, *Phys. Rev. C* **65**, 061601(R).
49. D. Cortina-Gil et al., *Phys. Lett. B* **529**, 36.
50. P.G. Hansen and B.M. Sherrill, *Nucl. Phys. A* **693**, 133.
51. J. Mortimer, I. J. Thompson, and J. A. Tostevin, Higher-order and E2 effects in medium energy ^{8}B breakup, *Phys. Rev. C* **65**, 064619.
52. A. M. Moro, J. M. Arias, J. Gomez-Camacho et al., Coupling to breakup channels using a transformed harmonic oscillator basis, *Phys. Rev. C* **65**, 011602.
53. F. M. Nunes and I. J. Thompson, Multistep effects in sub-Coulomb breakup, *Phys. Rev. C* **59**, 2652.
54. J. A. Tostevin, F. M. Nunes, and I. J. Thompson, Calculations of three-body observables in ^{8}B breakup, *Phys. Rev. C* **63**, 024617.
55. I.J. Thompson, J.A. Tostevin and F.M. Nunes, Multistep Coulomb and nuclear breakup of one-nucleon halo nuclei, *Nucl. Phys. A* **690**, 294.
56. B. Davids, Sam M. Austin, D. Bazin et al., Electromagnetic dissociation of ^{8}B and the rate of the ^{7}Be(p,γ)^{8}B reaction in the Sun, *Phys. Rev. C* **63**, 065806.
57. V.S. Melezhik and D. Baye, Nonperturbative time-dependent approach to breakup of halo nuclei, *Phys. Rev. C* **59**, 3232; Time-dependent analysis of the Coulomb breakup method for determining the astrophysical S factor, *Phys. Rev. C* **64**, 054612.
58. H. Esbensen and G. F. Bertsch, Eikonal approximation in heavy-ion fragmentation reactions, *Phys. Rev. C* **64**, 014608.
59. S. Typel and R. Shyam, Dynamical description of the breakup of one-neutron halo nuclei ^{11}Be and ^{19}C, *Phys. Rev. C* **64**, 024605.